Search for New Physics in All-hadronic Events with AlphaT in 8 TeV data at CERN

Yossof Eshaq

Submitted in Partial Fulfillment of the

Requirements for the Degree Doctor of Philosophy

Supervised by Professor Aran Garcia-Bellido

Department of Physics

Astronomy

Arts, Sciences and Engineering

University of Rocheser

September 29, 2014

Abstract

An inclusive search for supersymmetric processes that produce final states with jets and missing transverse energy is performed in pp collisions at a centre-of-mass energy of $\sqrt{s} = 8\,\text{TeV}$. The data sample corresponds to an integrated luminosity of 18.5 fb^{-1} collected by the CMS experiment at the LHC. In this search, a dimensionless kinematic variable, α_{T}, is used to discriminate between events with genuine and misreconstructed missing transverse energy. The search is based on an examination of the number of reconstructed jets per event, the scalar sum of transverse energies of these jets, and the number of these jets identified as originating from bottom quarks. The results are interpreted with various simplified models, with a special emphasis on models with a compressed mass spectrum.

0.1 Theoritical motivation

SM,Higgs,SUSY

Particle physics concerns itself with the study of particles and fields. Our current knowledge of their characterictics and interactions are formalized the quantum field theory called the Standard Model. I through three symmetries: The color charge symmetry of Quantum Chromo Dynamics (QCD) represented in SU(3), the flavor symemmetry of Quantum Flavor Dynamics (QFD) represented in SU(2) and the electric charge symmetry of Quantum Electro Dynamics represented in U(1). Together, SU(3)XSU(2)XU(1) represent the field theory.

0.2 LHC and CMS

LHC, CMS

0.3 Definition of $\alpha_{\mathbf{T}}$

0.4 Data sets and Monte Carlo samples

0.4.1 Data sets

The data analysed consist of the full run of 2012.

The following datasets are used to populate the hadronic signal and control samples. They correspond to the full data run of 2012 and an integrated luminosity of $19.45 \pm 0.8\,\text{fb}^{-1}$. The official JSON from the 22^{nd} Jan 2013 is used to filter only certified luminosity sections with the run range 190456–208686.

Table 1: Datasets.

Dataset	Luminosity (fb^{-1})
Hadronic	19.45
Muon	19.72
Photon	19.63

0.4.2 MC samples for signal and SM backgrounds

The SM background Monte Carlo samples for physics at 8 TeV are taken from the `Summer12` simulation production run with `CMSSW_5_3_X` with the `PU_S10` scenario. The effective luminosity of each MC sample is normalised to the integrated luminosity of the corresponding dataset, as listed in Table 2. The signal MADGRAPH Monte Carlo samples, listed in Table **??**, are taken from a `FastSim` simulation production based on `CMSSW_5_2_X`. All MC samples are reweighted on an event-by-event basis such that the distribution of pile-up (PU) interactions matches that observed in data. This is done using the recommended recipe and the PU JSON of 13^{th} December 2012.

Table 2: MC samples for Standard Model processes.

Sample	HT (GeV)	Cross section (pb)	Corrected Cross section (pb)
W $\to l\nu$	Inclusive	37509.0	34133.2
W $\to l\nu$	150 - 200	253.8	234.53
W $\to l\nu$	200 - 250	116.5	103.94
W $\to l\nu$	250 - 300	57.6	51.34
W $\to l\nu$	300 - 400	48.4	42.41
W $\to l\nu$	400 - ∞	30.8	26.36
Z $\to \nu\bar{\nu}$	50 - 100	452.8	405.21
Z $\to \nu\bar{\nu}$	100 - 200	190.4	173.76
Z $\to \nu\bar{\nu}$	200 - 400	45.1	42.41
Z $\to \nu\bar{\nu}$	400 - ∞	6.26	5.81
$t\bar{t}$	Inclusive	234.0	271.44
$Z/\gamma^* \to l^+l^-(m_{ll} > 50)$	Inclusive	3503.7	3258.45
$Z/\gamma^* \to l^+l^-(10 < m_{ll} < 50)$	Inclusive	13124.1	12205.4
$Z/\gamma^* \to l^+l^-$	200 - 400	24.3	22.24
$Z/\gamma^* \to l^+l^-$	400 - ∞	3.36	3.11
γ + jets	200 - 400	1140.8	1060.9
γ + jets	400 - ∞	124.7	115.97
WW	Inclusive	57.1	57.1
WZ	Inclusive	12.6	12.6
ZZ	Inclusive	8.26	8.26
t (t-channel)	Inclusive	56.4	56.4
$\bar{t}$ (t-channel)	Inclusive	30.7	30.7
t (s-channel)	Inclusive	3.79	3.79
$\bar{t}$ (s-channel)	Inclusive	1.76	1.76
t (tW-channel)	Inclusive	11.1	11.1
$\bar{t}$ (tW-channel)	Inclusive	11.1	11.1

0.4.3 Corrections to cross sections for SM samples

A simulated event is weighted by the total numer of events in the MC sample, the thoeritical cross section, and total luminosiy of the data being studied. The MC Pog provides next-to-next-to leading order (NNLO) thoeritical cross section for un-filtered (inclusive) SM samples [**?**]. In an attempt to provide higher statistics in tails of distrubtion analyses often cut on (ie $H_{\mathrm{T}}{}^{\mathrm{parton}}$, N^{parton}, $\hat{p}_T$), MC samples are provided binned in these variables. Only the leading-order (LO) cross sections are provided [**?**] but in general, the k-factors required to go from LO to NNLO cross sections are determined using corresponding inclusive samples and applied to each binned sample.

Studies conducted by other analyses [**?**] revealed that some LO cross sections calculated for MC samples binned according to $H_{\mathrm{T}}{}^{\mathrm{parton}}$ are inaccurate to a level as large as 10%, leading to non-physical discontinuities in the $H_{\mathrm{T}}{}^{\mathrm{parton}}$ distribution constructed from the binned samples of a

given process. Futhermore, due to an error in production, the $\mathrm{W} \to l\nu \quad H_{\mathrm{T}}$ binned samples exhibit H_{T}-depended biases. The following paragraphs describes a procedure to measure corrections to the discontinuites and biases of the $\mathrm{W} \to l\nu \quad {H_{\mathrm{T}}}^{\mathrm{parton}}$ binned samples as a function of H_{T}. Other analyses created similar procedures to correct the $\mathrm{Z} \to \mu\mu \quad {H_{\mathrm{T}}}^{\mathrm{parton}}$ binned samples, this analysis uses those measured corrections as k-factors.

As a first step, we wish to reweigh the cross sections of the ${H_{\mathrm{T}}}^{\mathrm{parton}}$ binned samples such that their ${H_{\mathrm{T}}}^{\mathrm{parton}}$ distributions match that of the inclusive sample's. Due to the inclusive sample's limited statitistics in the tails of H_{T} distribution, we instead use the N^{parton} binned's ${H_{\mathrm{T}}}^{\mathrm{parton}}$ distribution which is verified to agree well with the inclusive sample figure 1 (a). Additionally, to smooth statistical flucutations, both distributions are fitted using a double exponetional of the form $exp(a + b * x + c * x^{1.05})$ for $H_{\mathrm{T}} > 500\,\mathrm{GeV}$ figure 1 (b). The ratio of the distributions figure 1(c) is applied as ${H_{\mathrm{T}}}^{\mathrm{parton}}$ dependent event weight.

In the high-H_{T} and high-$\not\!\!E_{\mathrm{T}}$ corner of kinematic phase space of this analysis (and other SUSY analyses) the overall normalization of MC samples do not agree well with data. Therefore a data sideband in H_{T} is used to determine sample-specific corrections that are appropriate for the H_{T}-$\not\!\!E_{\mathrm{T}}$ phase space covered by this analysis. This correction is determined for the $\mathrm{W} \to l\nu$ and $t\bar{t}$ samples by impososing requirements on the number of muons, jets, and b-tagged jets, to obtain samples rich in W + jets, and $t\bar{t}$ events. A sideband in H_{T} is used to determine both the yields in data and MC expectations. The sideband is defined by the region $200 < H_{\mathrm{T}} < 225\,\mathrm{GeV}$ and uses the jet p_{T} thresholds $(73, 73, 37\,\mathrm{GeV})$ to maintain comparable jet multiplicities, kinematics. and background admixtures as observed for the higher HT bins. Trigger efficiency and b-tag scale factor corrections are determined and applied to the MC samples. The purity of the samples are $> 80\%$ and any contamination is taken into account. The correction is determined by taking the ratio of the data yield over the MC expectation in the sideband. Table 3 summarises the selection and corrections for the different samples.

Table 3: Correctins determined from a data sideband for the W + jets and $t\bar{t}$ samples. "Corrected yield" reflects the observed data yield minus the contamination as given by MC.

Process	Selection	Purity	Corrected yield	MC expectation	Correction Factor
W + jets	μ + jets, $2 \leq n_{\text{jet}} \leq 3$, $n_{\text{b}} = 0$	0.90	15682	18013.1 ± 85.9	0.87 ± 0.01
$t\bar{t}$	μ + jets, $n_{\text{jet}} \geq 2$, $n_{\text{b}} \geq 2$	0.83	752	736.7 ± 11.5	1.02 ± 0.05

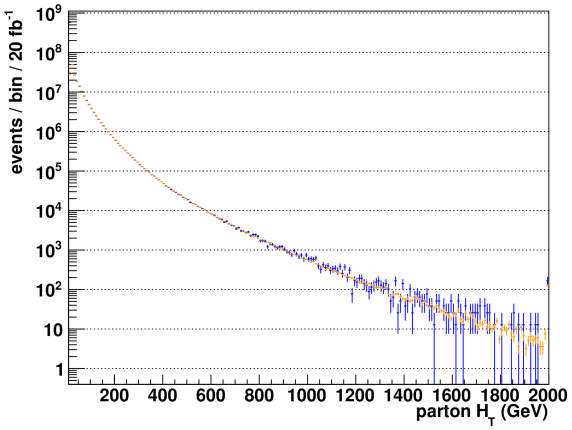

(a) Parton H_{T} distrbution for the $\mathrm{W} \to l\nu$ inclusive sample (blue) and $\mathrm{W} \to l\nu$ N^{parton} binned sample (orange.)

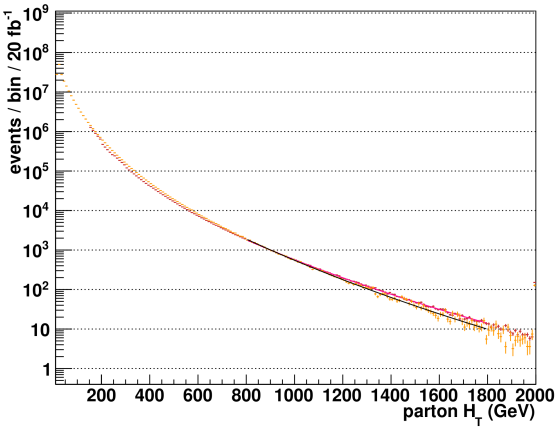

(b) Fitted Parton H_{T} distrbution for the $\mathrm{W} \to l\nu$ ${H_{\mathrm{T}}}^{\mathrm{parton}}$ sample (purple) and $\mathrm{W} \to l\nu$ N^{parton} binned sample (orange.)

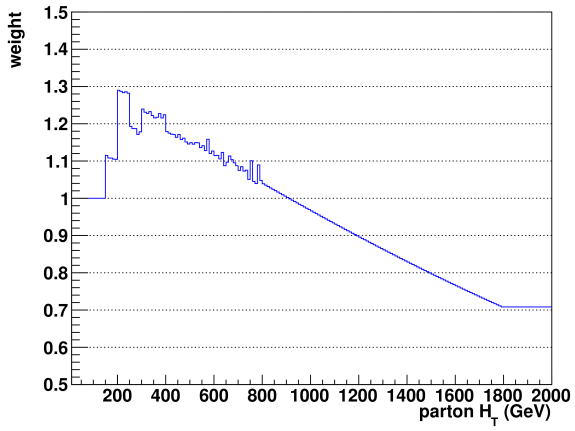

(c) Event weight determined from ration of figure 1 (b)

Figure 1: Generator-level ${H_{\mathrm{T}}}^{\mathrm{parton}}$ distributions and measured weights

0.5 Triggers

0.5.1 Hadronic signal region

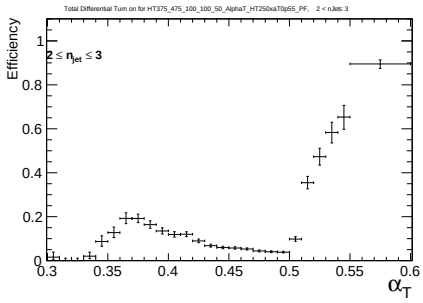

(a) Differential, $375 < H_{\mathrm{T}} < 475\,\mathrm{GeV}$

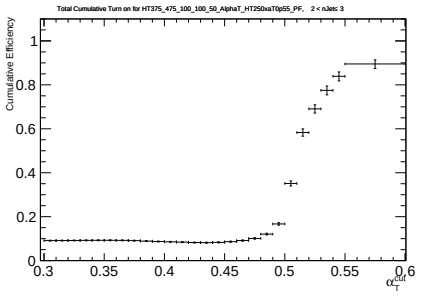

(b) Cumulative, $375 < H_{\mathrm{T}} < 475\,\mathrm{GeV}$

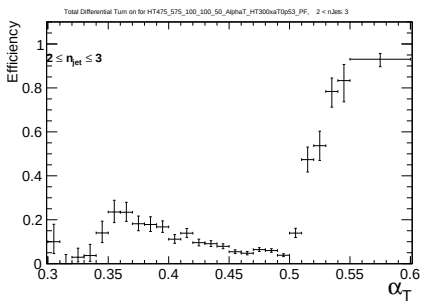

(c) Differential, $475 < H_{\mathrm{T}} < 525\,\mathrm{GeV}$

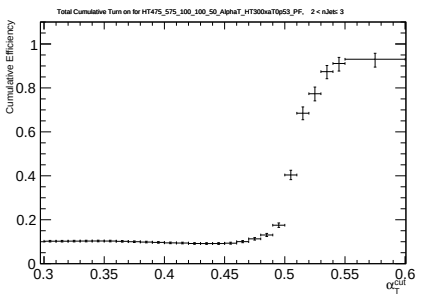

(d) Cumulative, $475 < H_{\mathrm{T}} < 525\,\mathrm{GeV}$

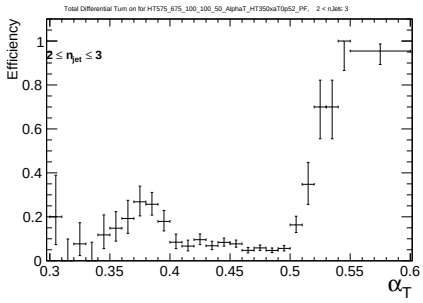

(e) Differential, $525 < H_{\mathrm{T}} < 675\,\mathrm{GeV}$

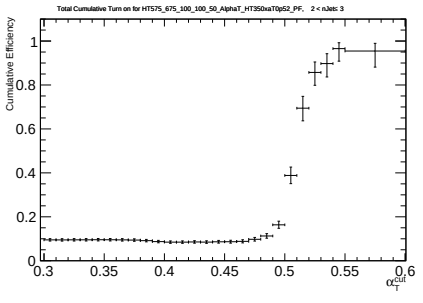

(f) Cumulative, $525 < H_{\mathrm{T}} < 675\,\mathrm{GeV}$

Figure 2: (Left) Differential and (Right) cumulative efficiency turn-on curves for the H_{T}-α_{T} cross triggers (as summarised in Table **??**) that record events for the three lowest H_{T} bins for events satisfying $2 \leq n_{\mathrm{jet}} \leq 3$.

0.5.2 Muon control samples

0.6 Physics objects

The definitions of the physics objects used in this analysis follow the recommendations of the various Physics Object Groups (POGs).

0.6.1 Jets

0.6.2 b-tagged jets

0.6.3 Muons

0.6.4 Photons

0.6.5 Electrons

0.6.6 Single isolated tracks

0.7 Event selection

0.7.1 Event vetoes for leptons, photons, and single isolated tracks

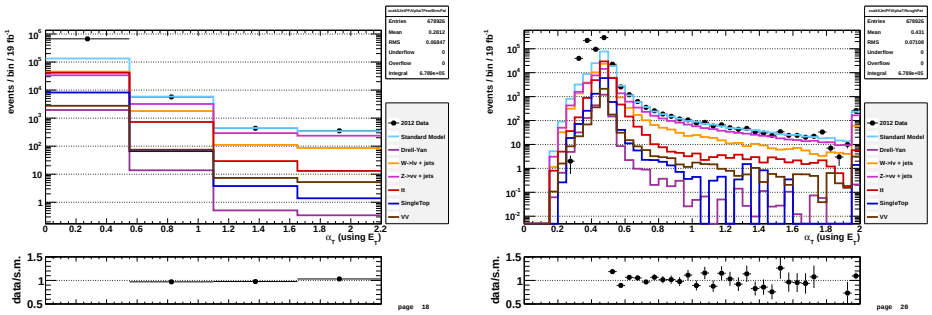

(a) (2–3,0) (b) (≥ 4,≥ 1)

Figure 3: Data–MC comparison of the α_{T} distribution for the hadronic signal region, following the application of the hadronic pre-selection criteria and the requirements $H_{\mathrm{T}} > 375\,\mathrm{GeV}$ and $\alpha_{\mathrm{T}} > 0.55$, for events satisfying (Left) $2 \leq n_{\mathrm{jet}} \leq 3$ and $n_{\mathrm{b}} = 0$ and (Right) $n_{\mathrm{jet}} \geq 4$ and $n_{\mathrm{b}} \geq 1$. Bands represent the uncertainties due to the limited size of MC samples.

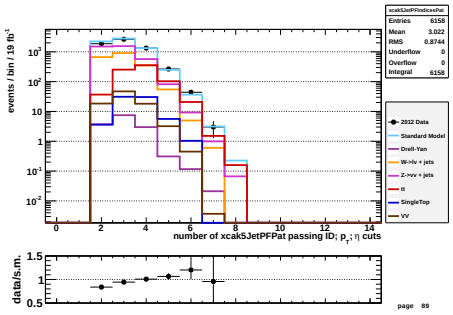

(a) n_{jet} distribution ($n_{\text{jet}} \geq 2$, $n_{\text{b}} \geq 0$).

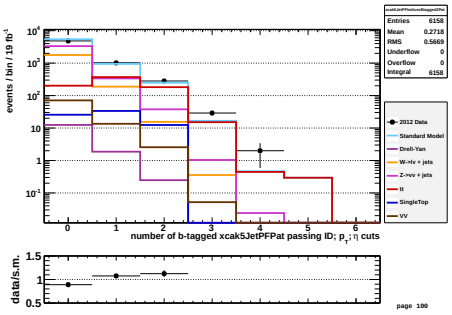

(b) n_{b} distribution ($n_{\text{jet}} \geq 2$, $n_{\text{b}} \geq 0$)

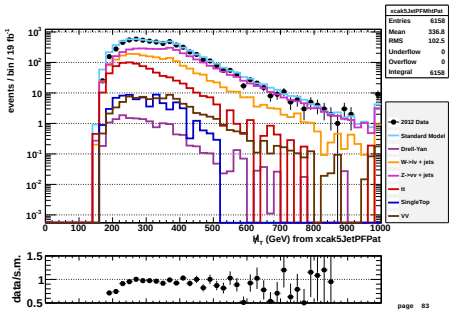

(c) H_{T} distribution ($n_{\text{jet}} \geq 2$, $n_{\text{b}} \geq 0$)

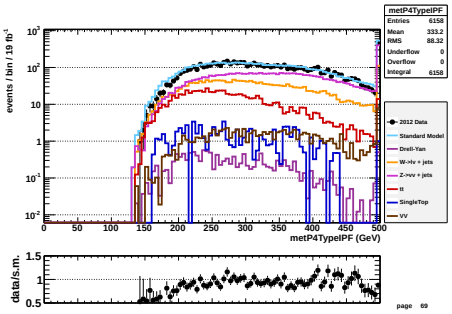

(d) H_{T} distribution ($n_{\text{jet}} \geq 2$, $n_{\text{b}} \geq 0$)

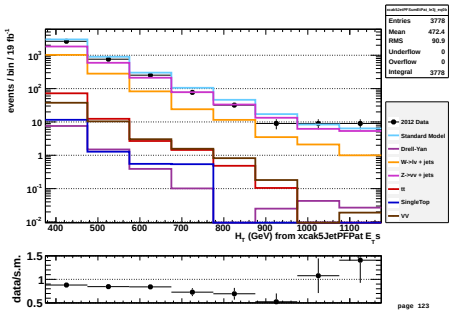

(e) H_{T} distribution ($2 \leq n_{\text{jet}} \leq 3$, $n_{\text{b}} = 0$)

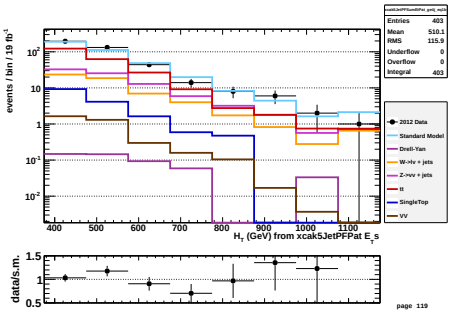

(f) H_{T} distribution ($n_{\text{jet}} \geq 4$, $n_{\text{b}} = 1$)

Figure 4: Data–MC comparisons of key variables for the hadronic signal region, following the application of the full signal region selection criteria and the requirements $H_{\text{T}} > 375\,\text{GeV}$ and $\alpha_{\text{T}} > 0.55$: (a) n_{jet}, (b) n_{b}, (c) H_{T}, and (d) $\not{E}_{\text{T}}$ distributions for an inclusive selection on n_{jet} and n_{b}, and (e,f) H_{T} for the two event categories ($2 \leq n_{\text{jet}} \leq 3$, $n_{\text{b}} = 0$) and ($n_{\text{jet}} \geq 4$, $n_{\text{b}} = 1$).

0.8 Background estimation for processes with genuine $\not{E}_{\mathrm{T}}$

0.9 Closure tests and systematic uncertainties on transfer factors

Limitations in simulating detector effects and event kinematics requires us to apply appropriate systematics uncertainties on the simulation-based translation factors. The following section describes how we obatain these systematic uncertainty through the method of closure tests.

0.9.1 Closure tests

At its core, the method compares an observed yield (N_{obs}) and a predicted yield (N_{pred}) in a subsample of a control region. The predicted yield is constructed by translating from a statisically independent data sample to the data sample of interest by the use of the proper translation factor. For example, for a given HT bin, a prediction for the $n_{\text{jet}} \geq 4$, n_{b} =1, μ + jets sample can be made by translating from the $2 \leq n_{\text{jet}} \leq 3$, n_{b} =1, μ + jets in data via the translation factor:

$$\frac{N_{\text{MC}}^{\mu+\text{jets}}(H_{\text{T}}, n_{\text{jet}} \geq 4, n_{\text{b}} = 1)}{N_{\text{MC}}^{\mu+\text{jets}}(H_{\text{T}}, 2 \leq n_{\text{jet}} \leq 3, n_{\text{b}} = 1)} \tag{1}$$

The agreement betwen N_{obs} and N_{pred} is expressed as $(N_{\text{obs}} - N_{\text{pred}})/N_{\text{pred}}$. Assuming only statistical uncertainties on N_{obs} and N_{pred}, deviation of the ratio from zero defines our level of closure. A closure test set is defined as ratios for each H_{T} bin. Looking at the ratio as a function of H_{T} allows the measurment of statistical significant biases from zero and/or any dependence on H_{T}. If statistically significant biases are observed, further studies are required to understand and correct for these biases.

Eight sets of closure tests probe key ingredients of the simulation modelling of the SM backgrounds with genuine $\not\!\!E_{\text{T}}$ as a function of H_{T}, as shown in Fig. 5. This is done for the two jet multiplicity bins separately: (a) $2 \leq n_{\text{jet}} \leq 3$ and (b) $n_{\text{jet}} \geq 4$.

Under the assumption of closure for the full ensemble of tests, systematic uncertainties on the transfer factors are derived for each n_{jet} category and H_{T} regions. The treatment for estimating the

systematic uncertainties on the transfer factors is described in Section 0.9.2.

As described in section ?? The α_{T} requirement is not imposed in the μ + jets control sample. Therfore it is important to verify the approach of using μ + jets samples without an α_{T} requirement to make background predictions in the signal region. The first set of closure tests (denoted by cirlces) attempts to do this by probing the modelling of the α_{T} distribution in genuine $\not\!\!E_{\mathrm{T}}$ events as a function of H_{T}. The tests compares data yields in the μ + jets sample with an α_{T} requirement against predictions determined in a μ + jets sample with the α_{T} requirement inverted.

The next three sets (triangles, crosses, squares) probe the sensitivity of the transfer factors to the relative admixture of events from the W + jets and $t\bar{t}$ processes. These tests are conservative, since by construction, the admixture changes little when translating from the μ + jets control region to the signal region, whereas the closure tests use sub-samples with different b-tag requirements and therfore have very different admixtures of W + jets and $t\bar{t}$ events. In the $2 \leq n_{\mathrm{jet}} \leq 3$ bin, the test is sub-divided into seperate jet categories. These tests also probe the modelling of the reconstruction of b-quark jets, although this also addressed more fully by dedicated studies that determine systematic uncertainties via the method described in Sec. **??**.

The remaining tests probe the simulation modelling of the jet multiplicity in the μ + jets and γ + jets samples, which is checked due to the exclusive binning in jet multiplicity. As in the case of the W + jets / $t\bar{t}$ admixture, this set of tests is a very conservative check, as predictions are always made from the same jet multiplicity bin, whereas the closure tests translate between the two bins.

Tables 4 and 5, which summarize the results obtained from fits of zeroeth order polynomials (i.e. a constant) to the sets of closure tests performed in the $2 \leq n_{\mathrm{jet}} \leq 3$ and $n_{\mathrm{jet}} \geq 4$ bins. Table 6 lists the fits result common to both jet multiplicites. The best fit value and its uncertainty is listed for each set of closure tests, along with the χ^2, the number of degrees of freedom, and the p-value of the fit. The best fit value for the constant parameter is indicative of the level of closure, as averaged across the full H_{T} range considered in the analysis, and the p-value is indicative of

whether there is any significant dependence on H_{T}.

The closure tests demonstrate, within the statistical precision of each test, that there are no significant biases or dependencies on H_{T} inherent in the transfer factors obtained from simulation.

One set of tests does indicate a poor goodness of fit (indicated by a low p-value), which is the $n_{\mathrm{b}} = 0 \rightarrow n_{\mathrm{b}} = 1$ test in the μ + jets sample for the $n_{\mathrm{jet}} \geq 4$ category, which has been identified as a upward (downward) fluctuation of event counts in the H_{T} bin 475–575 GeV (575–675 GeV) when $n_{\mathrm{b}} = 1$. Combining these two bins yields an acceptable fit result, as indicated in Table 5, which points to a simple fluctuation rather than any systematic bias.

In addition to the fits described above, linear fits are also performed. The best fit values for the slope terms and the p-values obtained from each fit are summarised in Tables 4, 5, and 6. Typically, the best fit values are of the order 10^{-4}, which corresponds to a percent-level change per 100 GeV.

Table 4: A summary of the results obtained from fits of zeroeth order polynomials (i.e. a constant) to four sets of closure tests performed in the $2 \leq n_{\mathrm{jet}} \leq 3$ bin.

		Constant fit			
Closure test	Symbol	Best fit value	χ^2	d.o.f.	p-value
$\alpha_{\mathrm{T}} < 0.55 \rightarrow \alpha_{\mathrm{T}} > 0.55$ (μ + jets)	Circle	0.007 ± 0.02	3.91	7	0.79
1 b-tags $\rightarrow$2 b-tags (μ + jets, nJet=3)	Triangle	-0.008 ± 0.04	3.20	7	0.87
0 b-tags $\rightarrow$1 b-tags (μ + jets, nJet=2)	Cross	0.111 ± 0.03	5.87	7	0.55
0 b-tags $\rightarrow$1 b-tags (μ + jets, nJet=3)	Square	0.040 ± 0.02	1.12	7	0.99

Table 5: A summary of the results obtained from fits of zeroeth order polynomials (i.e. a constant) to three sets of closure tests performed in the $n_{\mathrm{jet}} \geq 4$ bin. †Further explanation of this fit can be found in the text.

		Constant fit			
Closure test	Symbol	Best fit value	χ^2	d.o.f.	p-value
$\alpha_{\mathrm{T}} < 0.55 \rightarrow \alpha_{\mathrm{T}} > 0.55$ (μ + jets)	Circle	0.011 ± 0.04	5.81	7	0.56
1 b-tags $\rightarrow$2 b-tags (μ + jets)	Triangle	0.045 ± 0.03	9.36	7	0.23
0 b-tags $\rightarrow$1 b-tags (μ + jets)	Square	0.007 ± 0.03	25.30	7	0.00
0 b-tags $\rightarrow$1 b-tags (μ + jets)†	Square	0.009 ± 0.03	10.12	6	0.12

Table 6: A summary of the results obtained from fits of zeroeth order polynomials (i.e. a constant) to four sets of closure tests ($2 \leq n_{\text{jet}} \leq 3 \rightarrow n_{\text{jet}} \geq 4$) that probe the accuracy of the MC modelling of the n_{jet} distribution observed in data, using the three data control samples.

		Constant fit			
Closure test	Symbol	Best fit value	χ^2	d.o.f.	p-value
$2 \leq n_{\text{jet}} \leq 3 \rightarrow n_{\text{jet}} \geq 4$ (μ + jets, 1 b-tags)	Times	-0.053 ± 0.03	8.02	7	0.33
$2 \leq n_{\text{jet}} \leq 3 \rightarrow n_{\text{jet}} \geq 4$ (μ + jets, 1 b-tags)	Invert. Triangle	0.018 ± 0.04	6.23	7	0.51
$2 \leq n_{\text{jet}} \leq 3 \rightarrow n_{\text{jet}} \geq 4$ (μ + jets, 0 b-tags)	Star	0.034 ± 0.02	9.24	7	0.24
$2 \leq n_{\text{jet}} \leq 3 \rightarrow n_{\text{jet}} \geq 4$ (γ + jets, 0 b-tags)	Diamond	0.100 ± 0.04	12.20	7	0.09

0.9.2 Systematic uncertainties from closure tests

Once it is established that no significantly large bias or trend is observed for any set of closure tests, then systematic uncertainties are determined.

Systematics are determined for each H_{T} bin,as indicated in Table 7. For each H_{T} region, the systematic uncertainty is estimated by taking the quadrature sum of the weighted mean and sample variance for the closure tests within the given H_{T} region. This procedure yields the values quoted in Table 7.

The effect of uncertainties related to the modelling of b-quark jets in simulation on the transfer factors is found to be negligible, at the percent level as discussed in Section **??**, in comparison to the aforementioned n_{jet}- and H_{T}-dependent systematic uncertainties.

Table 7: A summary of the magnitude of the systematic uncertainties (%) assigned to the transfer factors, according to n_{jet} and H_{T} region.

	H_{T} region (GeV)							
n_{jet}	375–475	475–525	525–675	675–775	775–875	875-975	1075-1075	> 1175
2–3	6	6	7	12	12	17	17	17
$\geq$4	6	6	8	14	14	14	14	21

Figure 5 shows the sets of closure tests overlaid on top of grey bands that represent the H_{T}-dependent systematic uncertainties in Table 7. These systematic uncertainties are assumed to fully

uncorrelated between the different b jet multiplicity categories and also the seven H_{T} regions, which is a conservative approach given that one can expect some correlation between adjacent H_{T} bins (due to comparable kinematics). This approach of decorrelating the H_{T} regions should be contrasted against the fits shown in Figure **??** that do assume a correlated behaviour in H_{T}.

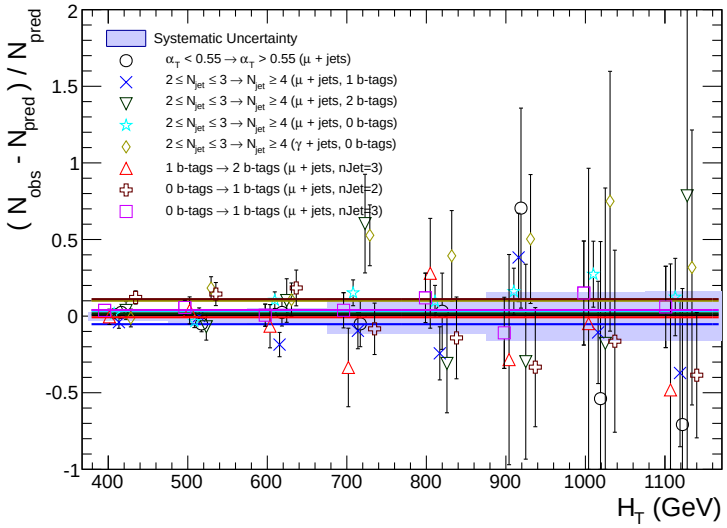

(a) $2 \le n_{\text{jet}} \le 3$

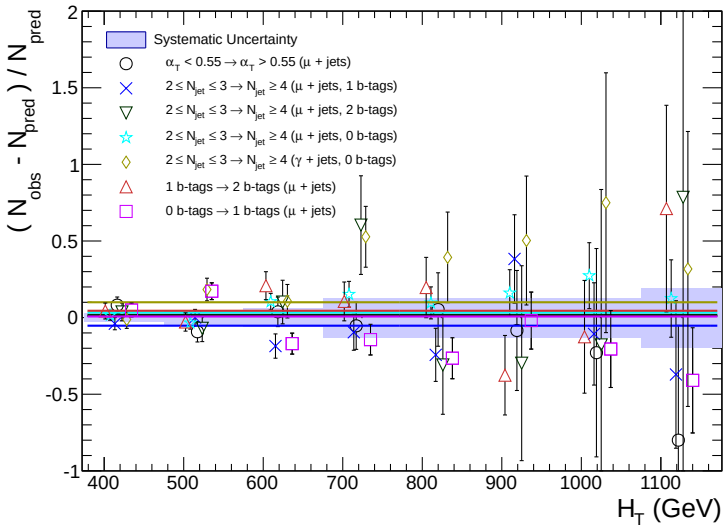

(b) $n_{\text{jet}} \ge 4$

Figure 5: Sets of closure tests (open symbols) overlaid on top of the systematic uncertainty used for each of the H_{T} region (shaded bands) and for the two different jet multiplicity bins: (a) $2 \le n_{\text{jet}} \le 3$ and (b) $n_{\text{jet}} \ge 4$.

0.10 Results

The likelihood described in ref:likelihood is used to relate yields, uncertainties. It is constructed using ROOTFIT [**?**] and maximized using MINUIT [**?**].

0.10.1 Standard Model

To test compatiblity with a Standard Model only hypothesis, the signal term is removed from the likelihood model. The parameter values maximizing the likelihood function are listed in Tables 9–14 found in Appendix .1. The resulting SM yields along with the observed data yields are summarized in Tables .2. The uncertainty on the yields are obtained by constructing a probability density function (p.d.f) from the maximized likelihood, then generating an ensemble of peudo-experiments from this p.d.f. and maxmizing the same likelihood form for each pseudo-experiment, resulting in an esemble of yields. The 68% quantile of each ensemeble defines the quoted uncertainty on the corresponding yield.

Figures 7–12 show the H_{T}-binned observed data yields (black filled circles) and the SM expectations and uncertainties (dark blue solid line with light blue bands) as determined by the fit for the hadronic signal region and the μ + jets or both (μ + jets,γ + jets) control samples, depending on the event category. The uncertainties in the SM expectations obtained from the ensemble of pseudo-experiments reflect the statistical uncertainties in the considered data samples and the systematic uncertainties in the transfer factors as discused in section 0.9. Figures 7–12 are summarized in tabular format in Tables 15–20 in appendix .2 along with observed data yields and the fit result for all event categories and both signal region and control sample bins.

For each n_{b}, n_{jet} category, the goodness-of-fit of the SM-only hypothesis is determined by considering simultaneously all H_{T} bins entering the likelihood. The goodness-of-fit described in [**?**] is obtained by comparing the nominal maximized likelihood value $L_{\mathrm{max}}^{\mathrm{data}}$ to the corresponding ensemble of values, L_{max}. The quantile which $L_{\mathrm{max}}^{\mathrm{data}}$ falls in the distributions is interpreted as a

p-value. A p-value derived from a chi-square is also plotted for comparison.

The p-values obtained, shown in Figure 6 (Left), are found to be uniformly distributed in the range 0.0–1.0, with the lowest p-value determined to be 0.17.

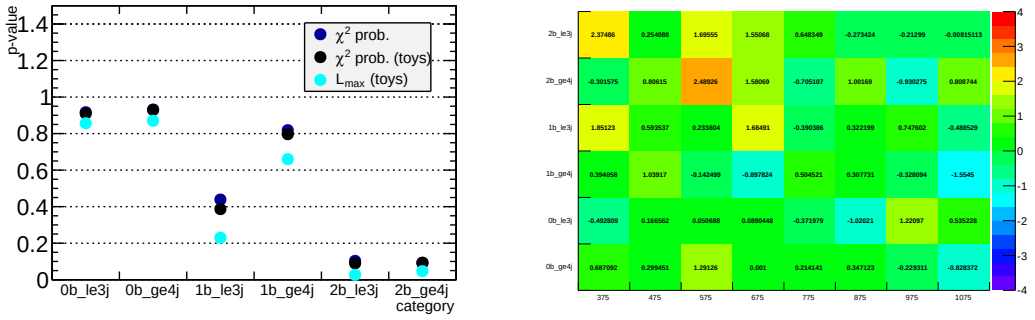

(a) p-values per event category.

(b) Pull versus signal region bin.

Figure 6: Pulls and p-values. See text for details

Table 8: Summary of hadronic yields from fit.

	375–475	475–575	575–675	675–775	775–875	875–975	975–1075	1075–∞
0b le3j SM	2637^{+50}_{-48}	759^{+24}_{-23}	252^{+14}_{-13}	$76.5^{+6.6}_{-4.7}$	$33.7^{+3.5}_{-3.7}$	$11.8^{+2.1}_{-2.3}$	$6.3^{+1.4}_{-1.2}$	$3.2^{+0.9}_{-0.9}$
0b le3j Data	2627	762	253	77	32	9	9	4
1b le3j SM	413^{+15}_{-14}	111^{+6}_{-4}	$35.8^{+3.4}_{-2.7}$	$10.1^{+1.6}_{-1.3}$	$3.7^{+0.8}_{-0.8}$	$1.6^{+0.6}_{-0.7}$	$0.5^{+0.3}_{-0.4}$	$0.1^{+0.1}_{-0.0}$
1b le3j Data	440	116	37	15	3	2	1	0
2b le3j SM	$63.0^{+3.9}_{-4.1}$	$18.0^{+1.3}_{-1.4}$	$4.2^{+0.6}_{-0.5}$	$1.1^{+0.2}_{-0.2}$	$0.2^{+0.1}_{-0.1}$	$0.0^{+0.0}_{-0.0}$	$0.0^{+0.0}_{-0.0}$	$0.0^{+0.0}_{-0.0}$
2b le3j Data	80	19	8	3	0	0	0	0
0b ge4j SM	460^{+16}_{-15}	298^{+12}_{-11}	146^{+7}_{-7}	$66.0^{+4.4}_{-5.5}$	$27.1^{+3.2}_{-3.5}$	$14.0^{+2.0}_{-1.9}$	$6.5^{+1.4}_{-1.5}$	$3.2^{+1.0}_{-1.0}$
0b ge4j Data	470	302	158	66	28	15	6	2
1b ge4j SM	192^{+9}_{-8}	122^{+6}_{-6}	$44.8^{+3.2}_{-3.7}$	$17.1^{+2.4}_{-2.0}$	$6.8^{+1.2}_{-1.3}$	$5.4^{+1.5}_{-1.5}$	$2.4^{+1.0}_{-0.8}$	$1.2^{+0.8}_{-0.8}$
1b ge4j Data	196	132	44	14	8	6	2	0
2b ge4j SM	$74.2^{+4.2}_{-4.4}$	$47.0^{+3.2}_{-3.3}$	$20.1^{+2.0}_{-1.8}$	$7.7^{+1.3}_{-1.1}$	$1.9^{+0.3}_{-0.3}$	$0.9^{+0.2}_{-0.2}$	$0.4^{+0.1}_{-0.1}$	$0.4^{+0.2}_{-0.1}$
2b ge4j Data	72	52	31	12	1	2	0	1

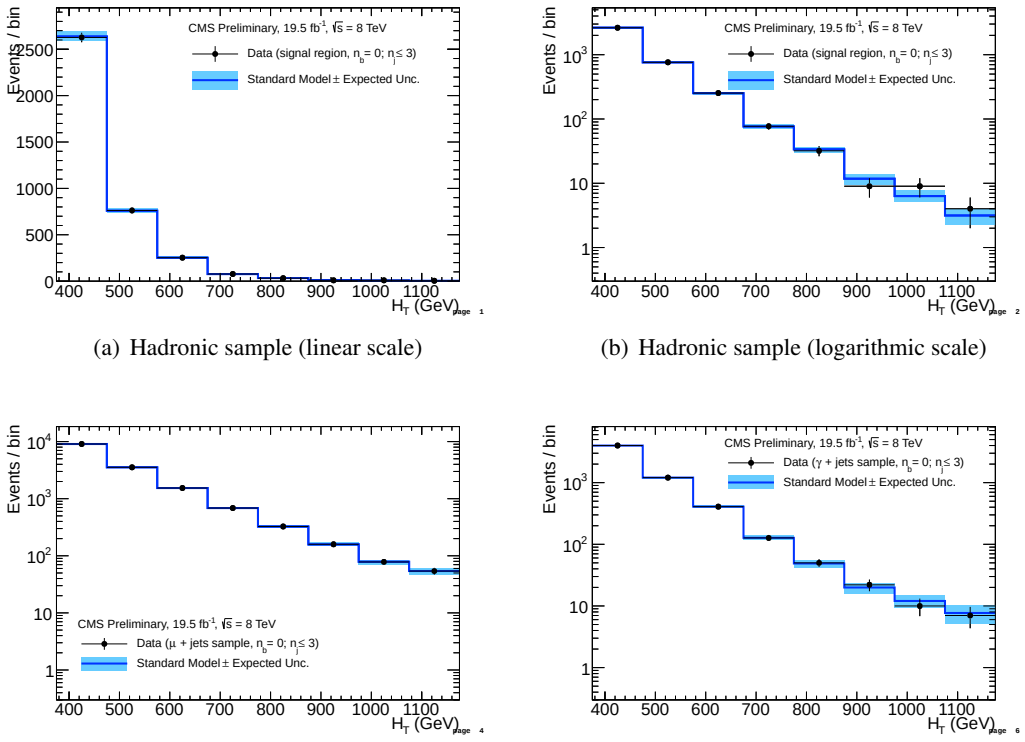

(a) Hadronic sample (linear scale)

(b) Hadronic sample (logarithmic scale)

(c) μ + jets sample

(d) γ + jets sample

Figure 7: Comparison of the H_{T}-binned observed data yields and SM expectations when requiring $2 \leq n_{\mathrm{jet}} \leq 3$ and $n_{\mathrm{b}} = 0$ for the (a-b) hadronic, (c) μ + jets, (d) $\mu\mu$ + jets and (e) γ + jets samples, as determined by a simultaneous fit to all data samples under the SM-only hypothesis. The observed event yields in data (black dots) and the expectations and their uncertainties (dark blue solid line with light blue bands), as determined by the simultaneous fit, are shown. For illustrative purposes only, the signal expectations (pink dashed line) for the model T2cc with $m_{\tilde{\mathrm{q}}} = 250\,\mathrm{GeV}$ and $m_{\mathrm{LSP}} = 240\,\mathrm{GeV}$ are stacked on top of the SM expectations.

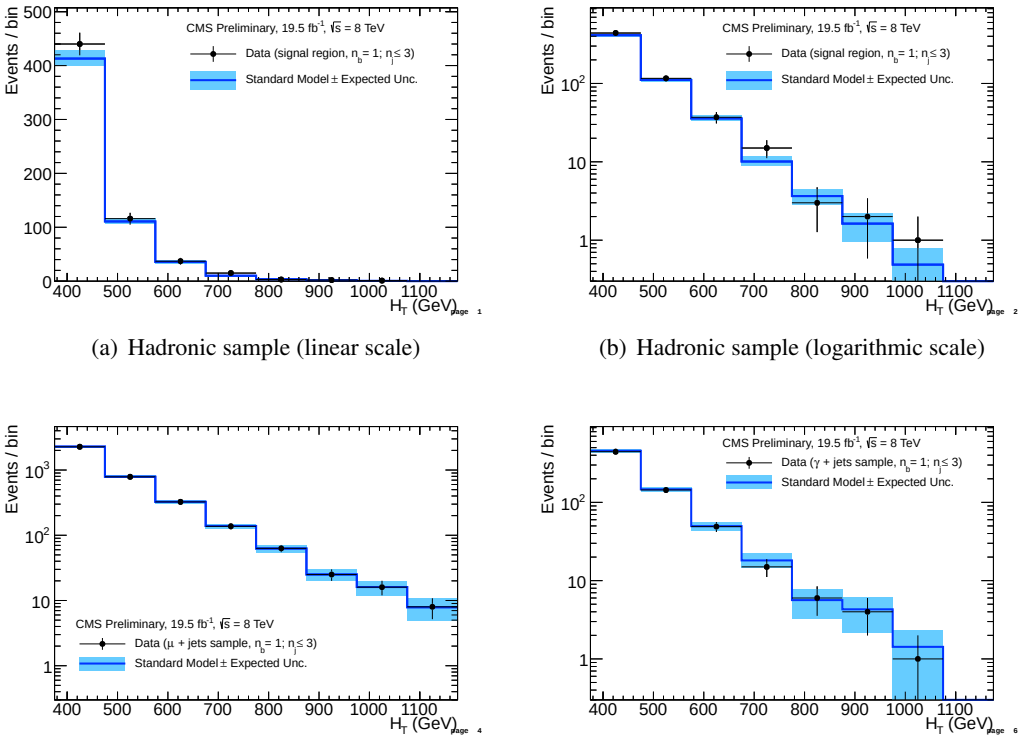

(a) Hadronic sample (linear scale)

(b) Hadronic sample (logarithmic scale)

(c) μ + jets sample

(d) γ + jets sample

Figure 8: Comparison of the H_{T}-binned observed data yields and SM expectations when requiring $2 \leq n_{\mathrm{jet}} \leq 3$ and $n_{\mathrm{b}} = 1$ for the (a-b) hadronic, (c) μ + jets, (d) $\mu\mu$ + jets and (e) γ + jets samples, as determined by a simultaneous fit to all data samples under the SM-only hypothesis. The observed event yields in data (black dots) and the expectations and their uncertainties (dark blue solid line with light blue bands), as determined by the simultaneous fit, are shown. For illustrative purposes only, the signal expectations (pink dashed line) for the model T2cc with $m_{\tilde{\mathrm{q}}} = 250\,\mathrm{GeV}$ and $m_{\mathrm{LSP}} = 170\,\mathrm{GeV}$ are stacked on top of the SM expectations.

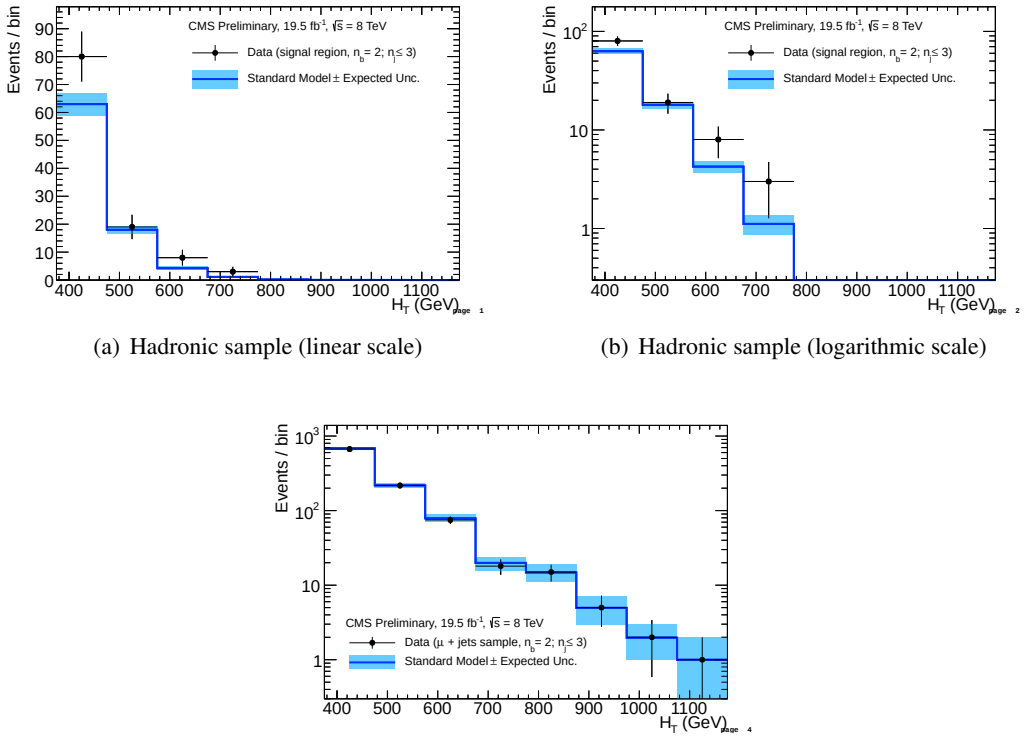

(a) Hadronic sample (linear scale)

(b) Hadronic sample (logarithmic scale)

(c) μ + jets sample

Figure 9: Comparison of the H_{T}-binned observed data yields and SM expectations when requiring $2 \leq n_{\mathrm{jet}} \leq 3$ and $n_{\mathrm{b}} = 2$ for the (a-b) hadronic and μ + jets samples, as determined by a simultaneous fit to both the hadronic and μ + jets data samples under the SM-only hypothesis. The observed event yields in data (black dots) and the expectations and their uncertainties (dark blue solid line with light blue bands), as determined by the simultaneous fit, are shown.

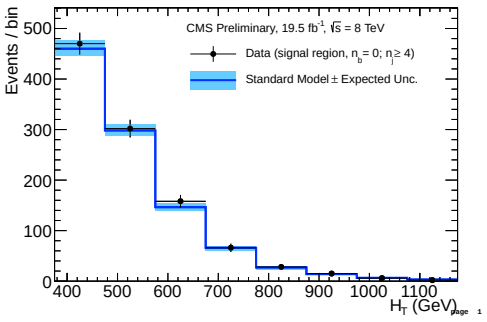

(a) Hadronic sample (linear scale)

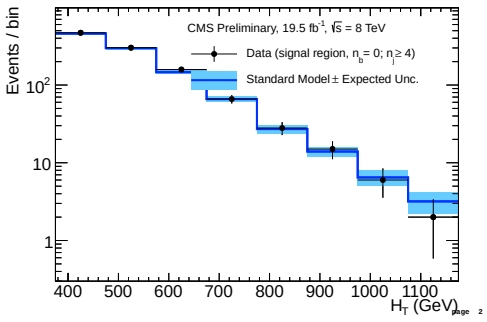

(b) Hadronic sample (logarithmic scale)

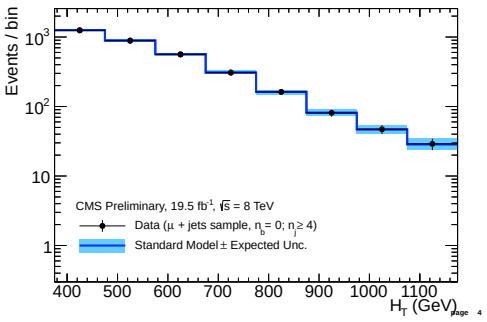

(c) μ + jets sample

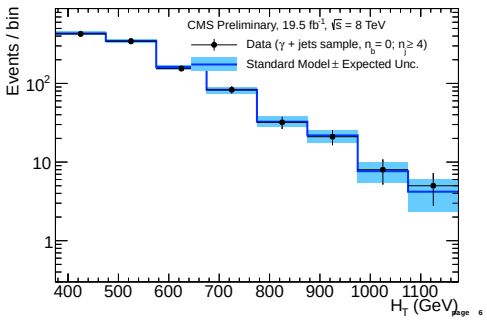

(d) γ + jets sample

Figure 10: Comparison of the H_{T}-binned observed data yields and SM expectations when requiring $n_{\mathrm{jet}} \geq 4$ and $n_{\mathrm{b}} = 0$ for the (a-b) hadronic, (c) μ + jets, (d) $\mu\mu$ + jets and (e) γ + jets samples, as determined by a simultaneous fit to all data samples under the SM-only hypothesis. The observed event yields in data (black dots) and the expectations and their uncertainties (dark blue solid line with light blue bands), as determined by the simultaneous fit, are shown. For illustrative purposes only, the signal expectations (pink dashed line) for the model T2cc with $m_{\tilde{\mathrm{q}}} = 250\,\mathrm{GeV}$ and $m_{\mathrm{LSP}} = 170\,\mathrm{GeV}$ are stacked on top of the SM expectations.

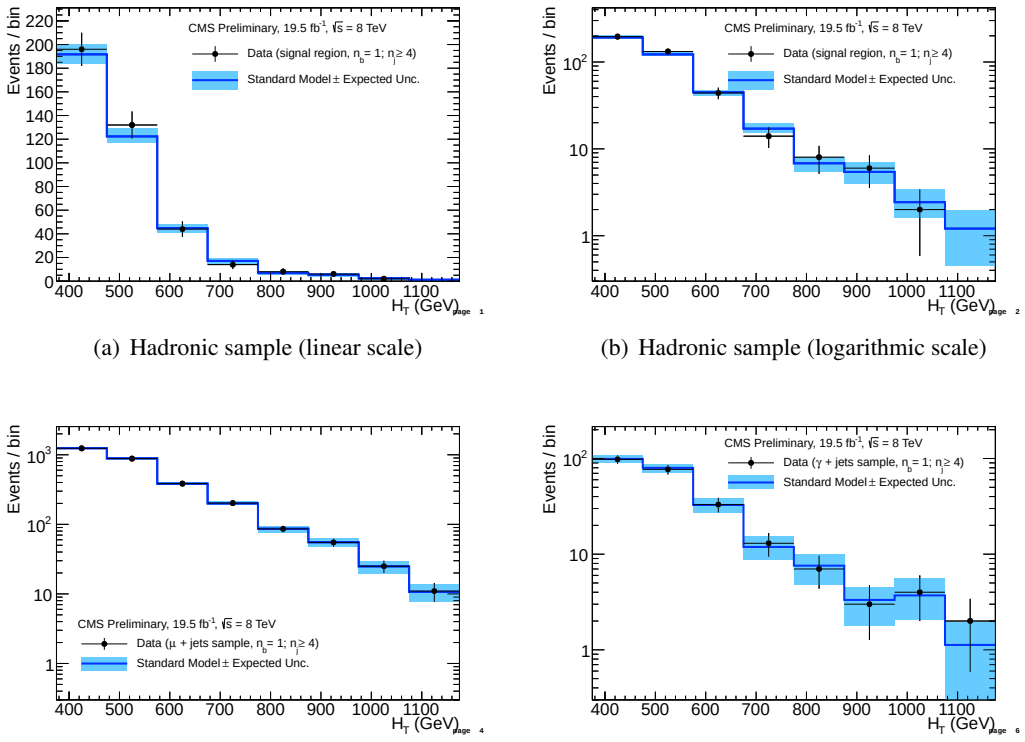

(a) Hadronic sample (linear scale)

(b) Hadronic sample (logarithmic scale)

(c) μ + jets sample

(d) γ + jets sample

Figure 11: Comparison of the H_{T}-binned observed data yields and SM expectations when requiring $n_{\mathrm{jet}} \geq 4$ and $n_{\mathrm{b}} = 1$ for the (a-b) hadronic, (c) μ + jets, (d) $\mu\mu$ + jets and (e) γ + jets samples, as determined by a simultaneous fit to all data samples under the SM-only hypothesis. The observed event yields in data (black dots) and the expectations and their uncertainties (dark blue solid line with light blue bands), as determined by the simultaneous fit, are shown. For illustrative purposes only, the signal expectations (pink dashed line) for the model T2cc with $m_{\tilde{\mathrm{q}}} = 250\,\mathrm{GeV}$ and $m_{\mathrm{LSP}} = 170\,\mathrm{GeV}$ are stacked on top of the SM expectations.

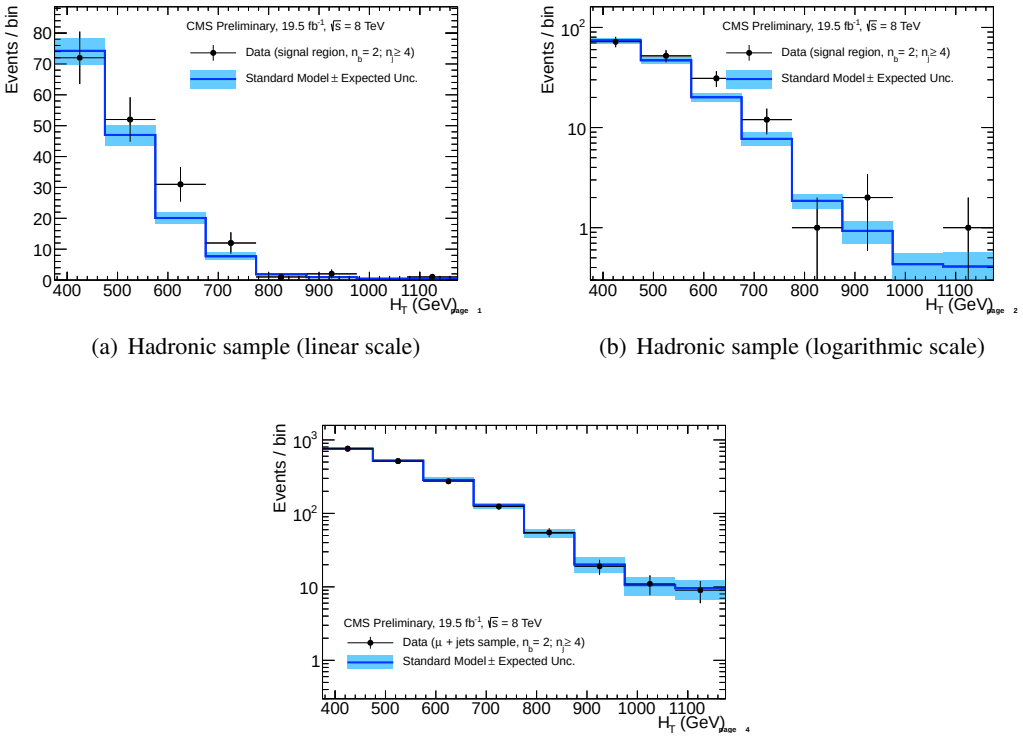

(a) Hadronic sample (linear scale)

(b) Hadronic sample (logarithmic scale)

(c) μ + jets sample

Figure 12: Comparison of the H_{T}-binned observed data yields and SM expectations when requiring $n_{\mathrm{jet}} \geq 4$ and $n_{\mathrm{b}} = 2$ for the (a-b) hadronic and μ + jets samples, as determined by a simultaneous fit to both the hadronic and μ + jets data samples under the SM-only hypothesis. The observed event yields in data (black dots) and the expectations and their uncertainties (dark blue solid line with light blue bands), as determined by the simultaneous fit, are shown.

.1 Maximum likelihood parameter values

Table 9: SM-only maximum-likelihood parameter values (0b le3j).

name	value	error
EWK^0	2.64e+03	4.7e+01
EWK^1	7.59e+02	2.2e+01
EWK^2	2.52e+02	1.1e+01
EWK^3	7.64e+01	6.0e+00
EWK^4	3.37e+01	3.5e+00
EWK^5	1.18e+01	2.0e+00
EWK^6	6.32e+00	1.4e+00
EWK^7	3.15e+00	8.9e-01
f^0_{Zinv}	0.64	0.02
f^1_{Zinv}	0.67	0.02
f^2_{Zinv}	0.70	0.02
f^3_{Zinv}	0.70	0.04
f^4_{Zinv}	0.69	0.04
f^5_{Zinv}	0.76	0.05
f^6_{Zinv}	0.76	0.06
f^7_{Zinv}	0.82	0.06
$\rho^0_{\mu W}$	1.01	0.05
$\rho^1_{\mu W}$	1.00	0.06
$\rho^2_{\mu W}$	1.00	0.07
$\rho^3_{\mu W}$	1.00	0.11
$\rho^4_{\mu W}$	1.01	0.11
$\rho^5_{\mu W}$	1.02	0.16
$\rho^6_{\mu W}$	0.98	0.15
$\rho^7_{\mu W}$	1.00	0.16
$\rho^0_{\gamma Z}$	1.02	0.04
$\rho^1_{\gamma Z}$	0.99	0.04
$\rho^2_{\gamma Z}$	1.00	0.06
$\rho^3_{\gamma Z}$	0.99	0.10
$\rho^4_{\gamma Z}$	1.02	0.11
$\rho^5_{\gamma Z}$	1.05	0.16
$\rho^6_{\gamma Z}$	0.95	0.14
$\rho^7_{\gamma Z}$	0.98	0.15

Table 10: SM-only maximum-likelihood parameter values (1b le3j).

name	value	error
EWK^0	4.13e+02	1.4e+01
EWK^1	1.11e+02	5.9e+00
EWK^2	3.58e+01	3.0e+00
EWK^3	1.01e+01	1.6e+00
EWK^4	3.66e+00	8.2e-01
EWK^5	1.63e+00	6.0e-01
EWK^6	4.87e-01	3.1e-01
EWK^7	1.21e-01	4.7e-02
f^0_{Zinv}	0.47	0.02
f^1_{Zinv}	0.55	0.03
f^2_{Zinv}	0.57	0.04
f^3_{Zinv}	0.64	0.07
f^4_{Zinv}	0.55	0.11
f^5_{Zinv}	0.81	0.08
f^6_{Zinv}	0.82	0.12
f^7_{Zinv}	0.00	0.83
$\rho^0_{\mu W}$	0.95	0.05
$\rho^1_{\mu W}$	0.99	0.06
$\rho^2_{\mu W}$	1.00	0.07
$\rho^3_{\mu W}$	0.98	0.11
$\rho^4_{\mu W}$	1.00	0.11
$\rho^5_{\mu W}$	1.00	0.16
$\rho^6_{\mu W}$	1.00	0.16
$\rho^7_{\mu W}$	1.00	0.16
$\rho^0_{\gamma Z}$	0.96	0.05
$\rho^1_{\gamma Z}$	0.99	0.06
$\rho^2_{\gamma Z}$	1.00	0.07
$\rho^3_{\gamma Z}$	0.96	0.11
$\rho^4_{\gamma Z}$	1.00	0.11
$\rho^5_{\gamma Z}$	0.99	0.15
$\rho^6_{\gamma Z}$	0.99	0.15
$\rho^7_{\gamma Z}$	1.00	0.16

Table 11: SM-only maximum-likelihood parameter values (2b le3j).

name	value	error
EWK^0	6.30e+01	3.8e+00
EWK^1	1.80e+01	1.5e+00
EWK^2	4.25e+00	5.4e-01
EWK^3	1.11e+00	2.7e-01
EWK^4	2.10e-01	5.9e-02
EWK^5	3.83e-02	1.8e-02
EWK^6	2.33e-02	1.7e-02
EWK^7	1.30e-03	1.3e-03
$\rho^0_{\mu W}$	0.94	0.05
$\rho^1_{\mu W}$	1.00	0.06
$\rho^2_{\mu W}$	0.98	0.07
$\rho^3_{\mu W}$	0.98	0.11
$\rho^4_{\mu W}$	1.00	0.11
$\rho^5_{\mu W}$	1.00	0.16
$\rho^6_{\mu W}$	1.00	0.16
$\rho^7_{\mu W}$	1.00	0.16

Table 12: SM-only maximum-likelihood parameter values (0b ge4j).

name	value	error
EWK^0	4.60e+02	1.6e+01
EWK^1	2.98e+02	1.2e+01
EWK^2	1.46e+02	8.2e+00
EWK^3	6.59e+01	5.7e+00
EWK^4	2.71e+01	3.3e+00
EWK^5	1.39e+01	2.2e+00
EWK^6	6.47e+00	1.5e+00
EWK^7	3.19e+00	9.5e-01
f^0_{Zinv}	0.52	0.02
f^1_{Zinv}	0.60	0.02
f^2_{Zinv}	0.61	0.03
f^3_{Zinv}	0.63	0.05
f^4_{Zinv}	0.71	0.05
f^5_{Zinv}	0.73	0.06
f^6_{Zinv}	0.74	0.07
f^7_{Zinv}	0.67	0.11
$\rho^0_{\mu W}$	0.98	0.05
$\rho^1_{\mu W}$	1.00	0.06
$\rho^2_{\mu W}$	0.97	0.07
$\rho^3_{\mu W}$	1.00	0.13
$\rho^4_{\mu W}$	1.00	0.13
$\rho^5_{\mu W}$	1.00	0.13
$\rho^6_{\mu W}$	1.00	0.13
$\rho^7_{\mu W}$	1.01	0.19
$\rho^0_{\gamma Z}$	0.98	0.05
$\rho^1_{\gamma Z}$	0.99	0.05
$\rho^2_{\gamma Z}$	0.96	0.07
$\rho^3_{\gamma Z}$	1.00	0.11
$\rho^4_{\gamma Z}$	0.99	0.12
$\rho^5_{\gamma Z}$	0.99	0.12
$\rho^6_{\gamma Z}$	1.01	0.13
$\rho^7_{\gamma Z}$	1.03	0.19

Table 13: SM-only maximum-likelihood parameter values (1b ge4j).

name	value	error
EWK^0	1.92e+02	8.5e+00
EWK^1	1.22e+02	6.1e+00
EWK^2	4.48e+01	3.5e+00
EWK^3	1.71e+01	2.1e+00
EWK^4	6.82e+00	1.3e+00
EWK^5	5.43e+00	1.5e+00
EWK^6	2.43e+00	7.9e-01
EWK^7	1.21e+00	6.3e-01
f^0_{Zinv}	0.23	0.02
f^1_{Zinv}	0.29	0.03
f^2_{Zinv}	0.38	0.05
f^3_{Zinv}	0.36	0.08
f^4_{Zinv}	0.49	0.10
f^5_{Zinv}	0.58	0.12
f^6_{Zinv}	0.70	0.11
f^7_{Zinv}	0.72	0.16
$\rho^0_{\mu W}$	0.99	0.05
$\rho^1_{\mu W}$	0.98	0.05
$\rho^2_{\mu W}$	1.00	0.07
$\rho^3_{\mu W}$	1.03	0.13
$\rho^4_{\mu W}$	0.99	0.13
$\rho^5_{\mu W}$	1.00	0.13
$\rho^6_{\mu W}$	1.00	0.13
$\rho^7_{\mu W}$	1.01	0.19
$\rho^0_{\gamma Z}$	1.00	0.06
$\rho^1_{\gamma Z}$	0.99	0.06
$\rho^2_{\gamma Z}$	1.00	0.08
$\rho^3_{\gamma Z}$	1.02	0.13
$\rho^4_{\gamma Z}$	0.99	0.13
$\rho^5_{\gamma Z}$	0.99	0.13
$\rho^6_{\gamma Z}$	1.01	0.13
$\rho^7_{\gamma Z}$	1.03	0.19

Table 14: SM-only maximum-likelihood parameter values (2b ge4j).

name	value	error
EWK^0	7.42e+01	4.4e+00
EWK^1	4.70e+01	3.1e+00
EWK^2	2.01e+01	1.8e+00
EWK^3	7.71e+00	1.1e+00
EWK^4	1.85e+00	3.4e-01
EWK^5	9.29e-01	2.3e-01
EWK^6	4.32e-01	1.4e-01
EWK^7	4.09e-01	1.5e-01
$\rho^0_{\mu W}$	1.01	0.05
$\rho^1_{\mu W}$	0.98	0.05
$\rho^2_{\mu W}$	0.94	0.07
$\rho^3_{\mu W}$	0.93	0.11
$\rho^4_{\mu W}$	1.01	0.13
$\rho^5_{\mu W}$	0.98	0.13
$\rho^6_{\mu W}$	1.01	0.13
$\rho^7_{\mu W}$	0.98	0.18

.2 SM-only yield tables

The following tables compare the observations in the hadronic and control samples with the maximum-likelihood expectations obtained by the SM-only fit.

Table 15: 0b le3j

H_{T} Bin (GeV)	375–475	475–575	575–675	675–775	775–875	875–975	975–1075	1075–∞
SM hadronic	2637^{+50}_{-48}	759^{+24}_{-23}	252^{+14}_{-13}	$76.5^{+6.6}_{-4.7}$	$33.7^{+3.5}_{-3.7}$	$11.8^{+2.1}_{-2.3}$	$6.3^{+1.4}_{-1.2}$	$3.2^{+0.9}_{-0.9}$
Data hadronic	2627	762	253	77	32	9	9	4
SM μ+jets	9074^{+82}_{-117}	3546^{+53}_{-60}	1538^{+36}_{-40}	686^{+21}_{-27}	325^{+17}_{-17}	158^{+12}_{-12}	$78.6^{+6.4}_{-8.5}$	$54.2^{+6.9}_{-7.6}$
Data μ+jets	9078	3545	1538	686	326	159	78	54
SM γ+jets	3993^{+59}_{-60}	1208^{+35}_{-35}	408^{+18}_{-20}	127^{+10}_{-9}	$48.8^{+6.2}_{-6.9}$	$19.9^{+3.5}_{-4.2}$	$12.0^{+3.0}_{-2.6}$	$7.7^{+2.5}_{-2.6}$
Data γ+jets	4000	1206	408	127	50	22	10	7

Table 16: 0b ge4j

H_{T} Bin (GeV)	375–475	475–575	575–675	675–775	775–875	875–975	975–1075	1075–∞
SM hadronic	460^{+16}_{-15}	298^{+12}_{-11}	146^{+7}_{-7}	$66.0^{+4.4}_{-5.5}$	$27.1^{+3.2}_{-3.5}$	$14.0^{+2.0}_{-1.9}$	$6.5^{+1.4}_{-1.5}$	$3.2^{+1.0}_{-1.0}$
Data hadronic	470	302	158	66	28	15	6	2
SM μ+jets	1254^{+35}_{-36}	889^{+31}_{-29}	567^{+22}_{-23}	308^{+17}_{-15}	162^{+10}_{-13}	$81.3^{+8.9}_{-8.5}$	$46.9^{+6.8}_{-7.0}$	$28.6^{+6.4}_{-4.9}$
Data μ+jets	1249	888	562	308	162	81	47	29
SM γ+jets	432^{+20}_{-20}	346^{+17}_{-16}	162^{+11}_{-12}	$83.0^{+7.1}_{-8.1}$	$32.6^{+5.5}_{-4.9}$	$21.8^{+3.7}_{-4.0}$	$7.7^{+2.2}_{-2.2}$	$4.2^{+1.9}_{-1.8}$
Data γ+jets	427	344	155	83	32	21	8	5

Table 17: 1b le3j

H_{T} Bin (GeV)	375–475	475–575	575–675	675–775	775–875	875–975	975–1075	1075–∞
SM hadronic	413^{+15}_{-14}	111^{+6}_{-4}	$35.8^{+3.4}_{-2.7}$	$10.1^{+1.6}_{-1.3}$	$3.7^{+0.8}_{-0.8}$	$1.6^{+0.6}_{-0.7}$	$0.5^{+0.3}_{-0.4}$	$0.1^{+0.1}_{-0.0}$
Data hadronic	440	116	37	15	3	2	1	0
SM μ+jets	2286^{+45}_{-45}	789^{+31}_{-26}	326^{+20}_{-16}	139^{+11}_{-11}	$62.7^{+8.0}_{-7.9}$	$25.1^{+4.7}_{-4.9}$	$16.1^{+4.0}_{-4.2}$	$7.9^{+3.0}_{-2.9}$
Data μ+jets	2272	787	325	137	63	25	16	8
SM γ+jets	457^{+23}_{-22}	147^{+11}_{-9}	$49.7^{+6.5}_{-5.5}$	$18.1^{+3.9}_{-3.6}$	$5.6^{+2.1}_{-2.4}$	$4.3^{+1.8}_{-2.2}$	$1.4^{+0.9}_{-1.4}$	$0.0^{+0.0}_{--0.0}$
Data γ+jets	444	144	49	15	6	4	1	0

Table 18: 1b ge4j

H_{T} Bin (GeV)	375–475	475–575	575–675	675–775	775–875	875–975	975–1075	1075–∞
SM hadronic	192^{+9}_{-8}	122^{+6}_{-6}	$44.8^{+3.2}_{-3.7}$	$17.1^{+2.4}_{-2.0}$	$6.8^{+1.2}_{-1.3}$	$5.4^{+1.5}_{-1.5}$	$2.4^{+1.0}_{-0.8}$	$1.2^{+0.8}_{-0.8}$
Data hadronic	196	132	44	14	8	6	2	0
SM μ+jets	1241^{+36}_{-33}	888^{+29}_{-26}	384^{+17}_{-20}	200^{+14}_{-11}	$86.6^{+9.0}_{-10.7}$	$55.3^{+7.8}_{-7.4}$	$24.9^{+4.6}_{-5.6}$	$10.7^{+3.1}_{-3.1}$
Data μ+jets	1238	881	385	202	86	55	25	11
SM γ+jets	$99.0^{+9.7}_{-8.7}$	$79.8^{+8.0}_{-8.7}$	$32.7^{+5.9}_{-5.3}$	$11.9^{+3.6}_{-3.1}$	$7.6^{+2.3}_{-2.8}$	$3.3^{+1.2}_{-1.6}$	$3.7^{+2.0}_{-1.6}$	$1.1^{+0.8}_{-1.1}$
Data γ+jets	98	77	33	13	7	3	4	2

Table 19: 2b le3j

H_{T} Bin (GeV)	375–475	475–575	575–675	675–775	775–875	875–975	975–1075	1075–∞
SM hadronic	$63.0^{+3.9}_{-4.1}$	$18.0^{+1.3}_{-1.4}$	$4.2^{+0.6}_{-0.5}$	$1.1^{+0.2}_{-0.2}$	$0.2^{+0.1}_{-0.1}$	$0.0^{+0.0}_{-0.0}$	$0.0^{+0.0}_{-0.0}$	$0.0^{+0.0}_{-0.0}$
Data hadronic	80	19	8	3	0	0	0	0
SM μ+jets	685^{+22}_{-29}	218^{+13}_{-14}	$78.8^{+9.4}_{-9.0}$	$19.9^{+4.0}_{-4.0}$	$14.8^{+4.1}_{-3.9}$	$5.0^{+2.0}_{-2.1}$	$2.0^{+1.0}_{-1.0}$	$1.0^{+1.0}_{-1.0}$
Data μ+jets	668	217	75	18	15	5	2	1

Table 20: 2b ge4j

H_{T} Bin (GeV)	375–475	475–575	575–675	675–775	775–875	875–975	975–1075	1075–∞
SM hadronic	$74.2^{+4.2}_{-4.4}$	$47.0^{+3.2}_{-3.3}$	$20.1^{+2.0}_{-1.8}$	$7.7^{+1.3}_{-1.1}$	$1.9^{+0.3}_{-0.3}$	$0.9^{+0.2}_{-0.2}$	$0.4^{+0.1}_{-0.1}$	$0.4^{+0.2}_{-0.1}$
Data hadronic	72	52	31	12	1	2	0	1
SM μ+jets	758^{+22}_{-26}	520^{+23}_{-21}	285^{+19}_{-17}	128^{+10}_{-11}	$54.1^{+7.0}_{-7.5}$	$20.1^{+4.8}_{-4.6}$	$10.6^{+3.1}_{-3.0}$	$9.6^{+2.9}_{-2.9}$
Data μ+jets	760	515	274	124	55	19	11	9

.3 Efficiencies and systematic uncertainties for simplified models

.3.1 T2cc

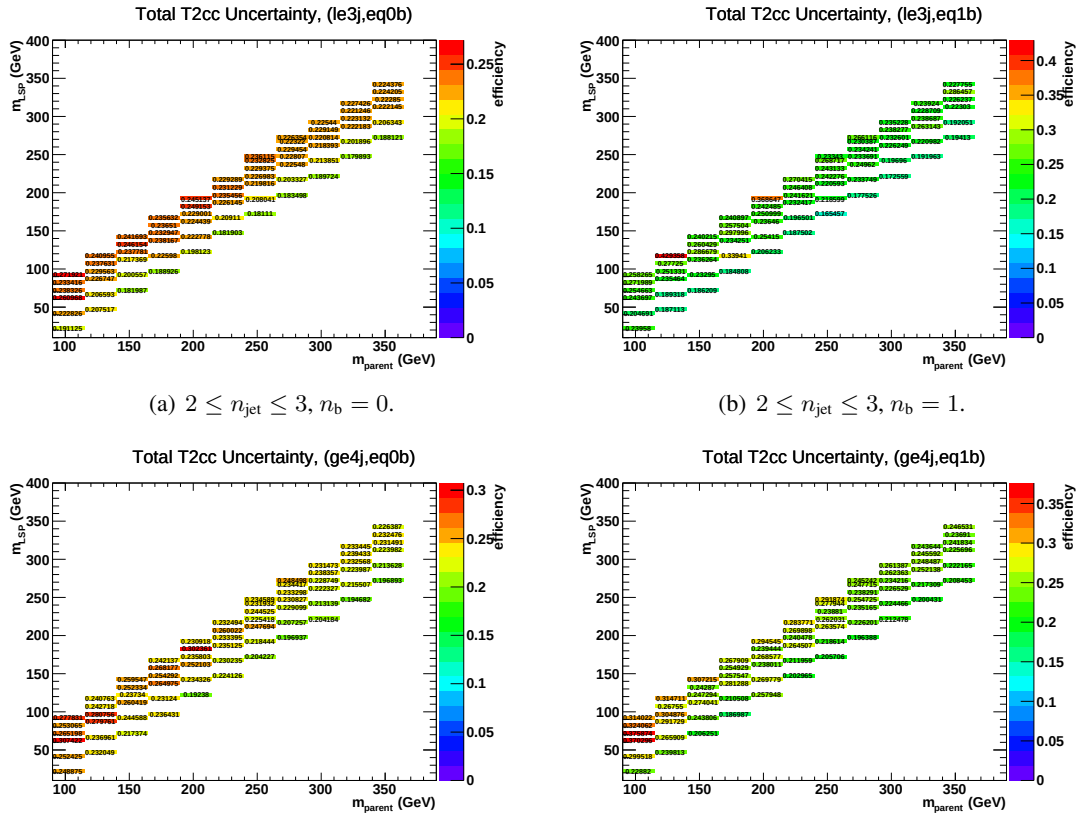

(a) $2 \leq n_{\text{jet}} \leq 3$, $n_{\text{b}} = 0$.

(b) $2 \leq n_{\text{jet}} \leq 3$, $n_{\text{b}} = 1$.

(c) $n_{\text{jet}} \geq 4$, $n_{\text{b}} = 0$.

(d) $n_{\text{jet}} \geq 4$, $n_{\text{b}} = 1$.

Figure 13: The total systematic uncertainty in the signal efficiency times acceptance for all relevant event categories for the T2cc intepretation.

.3.2 T2tt

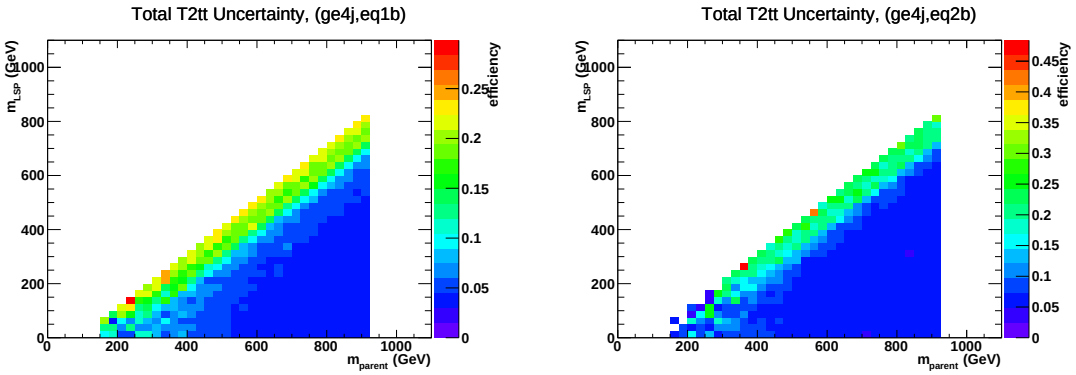

(a) $n_{\text{jet}} \geq 4$, $n_{\text{b}} = 1$.

(b) $n_{\text{jet}} \geq 4$, $n_{\text{b}} = 2$.

Figure 14: The total systematic uncertainty in the signal efficiency times acceptance for all relevant event categories for the `T2tt` intepretation.

Bibliography

[1] S. Chatrchyan et al. Missing transverse energy performance of the cms detector. *JINST*, 6:P09001, 2011.

[2] Serguei Chatrchyan et al. Determination of Jet Energy Calibration and Transverse Momentum Resolution in CMS. *JINST*, 6:P11002, 2011.

[3] V. Khachatryan et al. Search for Supersymmetry in pp Collisions at 7 TeV in Events with Jets and Missing Transverse Energy. *Phys. Lett. B*, 698:196, 2011.

[4] L. Randall and D. Tucker-Smith. Dijet searches for supersymmetry at the large hadron collider. *Phys. Rev. Lett.*, 101:221803, 2008.